Characteristics and dynamics of surfzone transverse finger bars

F. Ribas[1,2] and A. Kroon[3]

[1] Patches of transverse finger bars have been identified in the surf zone of Noordwijk beach (Netherlands). They consisted of three to nine elongated accumulations of sand attached to the low-tide shoreline. The bars extended up to 50 m into the inner surf zone, had an oblique orientation with respect to the shore-normal, and were quasiregularly spaced in the alongshore direction. We analyzed nearly 6 years of video data and observed a significant presence of finger bars (14% of the time with good data). Bars were visible on 193 days, gathered in 44 events that persisted from 2 days to 2 months. Obliquely incident waves of intermediate and approximately constant height were dominant during finger bar presence. Shore-normal incident or more energetic wave fields destroyed the bar patches. The underlying bathymetry affected finger bar formation: inner surfzone troughs with cross-shore areas of 100 m^2 and inner surfzone slopes of 0.02 were more conducive to their growth. The mean alongshore wavelength of the finger bar patches was 39 m, ranging from 21 to 75 m. Bar crests deviated up to 40 degrees from the shore-normal against the alongshore current direction ("up-current orientation") and bar patches migrated at rates up to 22 m/day in the direction of the alongshore current. We used these observations to test existing theoretical self-organization mechanisms for transverse bar formation. The "bed-flow mechanism" was the most viable explanation for the generation and persistence of Noordwijk finger bars. Our observations were consistent with most of the predictions of two models that included this interaction, but migration rates differed by 1 order of magnitude.

1. Introduction

1.1. Field Observations of Transverse Finger Bars

[2] Transverse finger bars are elongated accumulations of sand that extend in the subtidal domain of some beaches up to a few meters depth, and have an orientation perpendicular or oblique with respect to the shore-normal (see Figure 1 and Table 1). Patches of several finger bars sometimes show a remarkable alongshore periodicity at intermediate length scales (15–200 m). The finger bars have different characteristics and origin from the transverse bars in classification schemes of beaches (for example, those in the "Transverse bar and rip state" of *Wright and Short* [1984]). The latter are much wider and less elongated and they develop when the horns of a preexisting crescentic bar weld to the beach. In such a scenario the most prominent features are deep and narrow rip channels alternating with the bars at length scales similar to finger bars [see *Holman et al.*, 2006, and references therein].

[3] The term transverse finger bars was first introduced by *Niederoda and Tanner* [1970] to refer to thin and long-crested bars that were not linked to the previous existence of any crescentic bar [*Komar*, 1998]. Patches of tens of bars often occur on microtidal sheltered coasts under low-energy wave conditions ($H_{rms} < 0.20$ m, where H_{rms} is the root mean square wave height). These beaches are wide, terraced, gently sloping ($\beta < 0.01$, with β being the mean beach slope) and they receive a large sediment supply. In such protected environments, the finger bars are very elongated (long-crested) and extend well outside the surf zone. Their cross-shore span or elongation, Δx, is 2–5 times larger than their wavelength, λ (the alongshore distance between two consecutive bars in a patch) and they show very low migration rates. For instance, *Gelfenbaum and Brooks* [2003] reported a maximum rate of 20 m/yr.

[4] The study of *Konicki and Holman* [2000] was pioneering in describing transverse finger bars along a more energetic open coast (the ocean beach of Duck, U.S.A., with a mean annual $H_{rms} = 0.64$ m). The Duck finger bars showed significantly smaller cross-shore spans and much larger migration rates than those observed in sheltered environments (see Table 1). In order to differentiate these two types of features and to emphasize the fact that significant wave breaking occurs over finger bars in open environments, the latter will be called "surfzone transverse finger bars."

[1]Institut de Ciències del Mar, CSIC, Barcelona, Spain.
[2]Also at Institute for Marine and Atmospheric research Utrecht, Utrecht University, Utrecht, Netherlands.
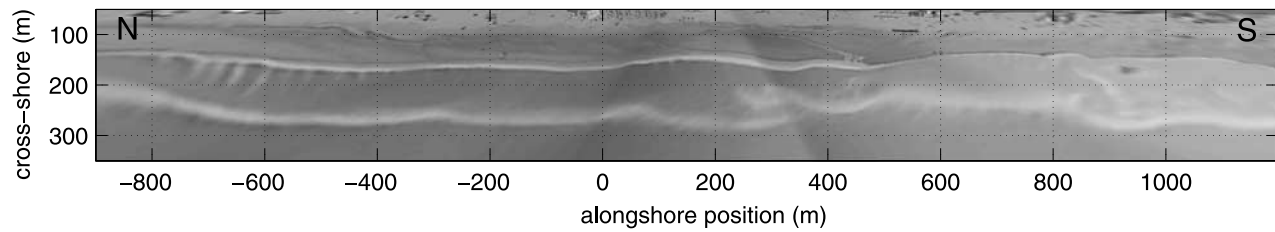[3]Geografisk Institut, Københavns Universitet, Copenhagen, Denmark.

Figure 1. Time-exposure planview image of Noordwijk on 27 August 2002, at 1300 GMT (low-tide conditions). A patch of surfzone transverse finger bars can be seen at $y = [-775, -400]$ m and $x = 180$ m, attached to the low-tide shoreline.

Konicki and Holman [2000] reported the existence of two types of surfzone finger bars: "trough bars," attached to the low-tide shoreline, and "offshore bars," seaward attached to a shore-parallel inner bar. They used 10 years of hourly measured video data to analyze bar statistics. Trough bars were visible 16 days per year on average, with a mean wavelength of 79 m. Offshore bars appeared 11 days per year with a wavelength of 172 m. The bar patches consisted of 1 to 4 bars and persisted from 1 day to 3 months. Crests of trough (offshore) bars deviated 32° (43°) from the shore-normal. *Konicki and Holman* [2000] conducted detailed bathymetric surveys and confirmed that the transverse stripes of foam detected in the video images corresponded to topographic features. Remarkably, no other long-term systematic measurements of surfzone transverse finger bars have been published so far.

1.2. Physical Mechanisms for Bar Development

[5] The emergence of nearshore rhythmic morphology has been often related to the sediment transport induced by standing low-frequency edge waves ("template mechanisms," [see *Komar*, 1998]). However, the requirements for the incident wave field that could explain the existence of a standing edge wave with a preferred wavelength are unrealistic in the stochastic forcing of surf zones in open beaches. Alternatively, "self-organization mechanisms" are based on the concept of morphodynamic instability, which can occur whenever the incident wave field and the associated alongshore current interact with the underlying erodible bed. If a positive feedback is established between certain developing features (like a patch of finger bars) and the associated flow and sand transport, the bar patch will eventually grow. Several self-organization models for surfzone finger bar formation and evolution, which include the combined effects of waves and currents, have been developed in the last decade. Most of them are based on Linear Stability Analysis (LSA), a method that describes growth of bars of infinitesimal height and indicates the

initial tendency of the system [*Christensen et al.*, 1995; *Ribas et al.*, 2003; *Calvete et al.*, 2005]. Nonlinear models are used in order to reproduce the finite amplitude features and study the long-term evolution [*Caballeria et al.*, 2002; *Garnier et al.*, 2006].

[6] The results of all these works demonstrate that morphodynamic feedback between the topography, the waves, the currents and the sand transport can be responsible for the formation and evolution of surfzone finger bars. Some model predictions are consistent in the majority of these studies and modeled features resemble finger bars in natural beaches. However, a serious limitation of our present knowledge of finger bars is the lack of quantitative comparisons between model results and field data. Moreover, recent studies have revealed that several theoretical aspects remain unsolved. Some essential characteristics of the modeled features, like their shape and the related timescales, significantly depend on the specific description used for the wave transformation and the sediment transport [*Klein and Schuttelaars*, 2005; *Ribas et al.*, 2005; *van Leeuwen et al.*, 2006]. Long-term systematic measurements of surfzone finger bars patches, including a detailed description of wave and bathymetric conditions, are essential to clarify the remaining open questions and improve our understanding of the physical processes.

1.3. Present Study

[7] The aim of the present contribution is to obtain quantitative field information about the development of surfzone transverse finger bars in order to better understand the underlying physics. Section 2 synthesizes the results of self-organization models into testable predictions. We use 6 years of hourly video images from Noordwijk beach (the Netherlands) to detect patches of finger bars. Sections 3 and 4 describe the field site and the methodology used and section 5 reports the observed characteristics of finger bars. We pay special attention to the wave and tide conditions and to the morphologic boundary conditions leading to bar

Table 1. Examples of Field Observations of Transverse Finger Bar Patches, Ordered by Year of Publication[a]

Site	H_{rms}, m	Tide, m	d_{50}, mm	β	λ, m	Δx, m	c_m, m/d	References
St. James Island, USA	0.06	0.5	0.41	0.003	64−218	640	0	*Niederoda and Tanner* [1970]
Duck beach, USA[b]	0.64	1.0	0.18	0.013	12−179	50	40	*Konicki and Holman* [2000]
Anna Maria Island, USA	0.18	0.7	0.50	0.002	75−120	4000	0.05	*Gelfenbaum and Brooks* [2003]
Como beach, Australia	0.19	0.6	0.50	0.005	40−80	200	−	*Eliot et al.* [2006]

[a]Here H_{rms} is the annual mean root mean square height, d_{50} is the mean grain size, β is the mean slope, λ is the wavelength, Δx is the maximum cross-shore span, and c_m is the maximum migration rate detected.
[b]The given length scales and migration rates correspond to the "trough bars."

Table 2. Surfzone Finger Bar Characteristics Predicted by Some Self-Organization Models[a]

θ	C_{di}	Orientation	λ	Migration Direction	Migration Rate	Dominant Coupling	References[b]
0°	increasing seaward	shore-normal	0.5 X_b	–	0 m/d	bed-surf	1, 2
>15°	approximately constant	up-current	0.5–3 X_b	down-flow	50–100 m/d	bed-flow	2, 3
<30°	increasing seaward	down-current	1–2 X_b	down-flow	0–200 m/d	bed-surf/bed-flow	2, 3

[a]Here θ is the offshore angle of wave incidence with respect to shore-normal, C_{di} is the cross-shore distribution of the depth-integrated sediment concentration, λ is the wavelength, and $X_b \propto H_{rms}/\beta$ is the surf zone width.

[b]Numbers correspond to the following references: 1, *Caballeria et al.* [2002], *Calvete et al.* [2005], and *van Leeuwen et al.* [2006]; 2, *Garnier et al.* [2006]; and 3, *Ribas et al.* [2003].

formation and development. Section 6 contains a discussion with specific emphasis on a comparison between the surfzone finger bars of Noordwijk and those detected at Duck. Finally, section 7 uses the field observations to test the predictions of existing self-organization models.

2. Predictions of Self-Organization Models

[8] Several self-organization models for nearshore bar formation have been reported in the last decade [*Christensen et al.*, 1995; *Caballeria et al.*, 2002; *Ribas et al.*, 2003; *Calvete et al.*, 2005; *Klein and Schuttelaars*, 2005; *Garnier et al.*, 2006; *van Leeuwen et al.*, 2006]. Table 2 lists the characteristics of the topographic patterns predicted by some of these models. A distinctive property of the modeled bar patches is the orientation of their bar crests with respect to the shore-normal. Three possibilities are distinguished: (1) exactly shore-normal orientation, (2) up-current orientation, where crests deviate from the shore-normal against the alongshore current, and (3) down-current orientation, where crests deviate in the down-flow direction. The orientation yielded by the models of Table 2 essentially depends on the angle of wave incidence and on the cross-shore distribution of the depth-integrated suspended sediment concentration in the surf zone. In all cases, these models predict a relationship between the wavelength and the surfzone width, $X_b \propto H_{rms}/\beta$. Considering X_b ranging from 50 to 200 m, modeled λ can vary from 25 to 600 m. Migration of bar patches is always in the direction of the alongshore current at rates up to a few hundreds of meters per day. Model results also establish that wave fields of relatively constant height during at least half a day are needed to create the bars.

[9] Models in Table 2 emphasized the role of two interactions between the bed and the hydrodynamics that can lead to surfzone bar formation: the "bed-surf coupling" and the "bed-flow coupling." These mechanisms usually compete with other processes of the complex surf zone but, under certain circumstances, one of them can be predominant and become a viable explanation for the growth and the characteristics of certain type of bars. In case of shore-normal waves ($\theta = 0°$, where θ is the offshore angle of wave incidence with respect to the shore-normal), the "bed-surf coupling" is dominant and can explain the formation of shore-normal finger bars (and of crescentic bars [see *Caballeria et al.*, 2002; *Calvete et al.*, 2005; *van Leeuwen et al.*, 2006]). The growing bars/shoals in the surf zone modify locally the incident wave field (the breaking intensity increases and small onshore currents are created) in such a way that their growth is reinforced. This positive feedback only occurs if the depth-integrated sediment concentration, C_{di}, increases rapidly with distance from shore because this enhances the convergence of sediment flux in onshore directed flows. This is verified in most of the available sediment transport formulations, where C_{di} is assumed to be a result of the shear stresses created by wave orbital velocities and mean currents.

[10] In case of oblique wave incidence, surfzone bars do not only change the wave transformation but also produce a deflection of the existing alongshore current. The latter process is predominant for very oblique wave incidence, $\theta > 30°$, and explains the growth of up-current oriented bars [*Ribas et al.*, 2003; *Garnier et al.*, 2006]. As a consequence of water mass conservation, the alongshore current veers toward the direction of maximum topographic gradient, hence offshore deflection occurs over up-current oriented bars. In order to get convergence of sediment flux over such bars, an approximately constant cross-shore distribution of C_{di} is required. This can occur in the inner surf zone of some beaches owing to the presence of bores and hydraulic jumps, for instance.

[11] In general, very complex sediment transport processes occur and interact inside the surf zone and the resulting sediment dynamics, including the distribution of C_{di}, is still poorly understood [*Komar*, 1998]. In case of intermediate wave incidence angles ($\theta < 30°$), the bed-flow and the bed-surf mechanisms compete and model results are less conclusive. In particular, the models included in Table 2 predict the formation of bars whose orientation depends on the distribution of C_{di}.

[12] The assumptions behind the existing self-organization models for finger bar formation limit the comparison of their results with observations on natural beaches. In LSA models, finger bar formation is assumed to occur over alongshore uniform beach bathymetries under constant wave conditions [*Ribas et al.*, 2003; *Calvete et al.*, 2005; *van Leeuwen et al.*, 2006]. They describe the stability properties of a profile, which is assumed to be representative of the whole bathymetry, and in case it is unstable, the initial tendency of the sea bed. The analysis yields the wavelength, shape, growth rate and migration speed of different topographic features and the one growing fastest is expected to emerge. By definition, the finger bar patches that are predicted to grow by LSA consist of an infinite number of equally spaced bars of infinitesimal amplitude. Otherwise, natural beaches show nonuniform bathymetries that are seldom in equilibrium with wave conditions, the latter being highly variable. The observed patches consist of a finite number of bars of a certain finite amplitude and a significant variability can be detected in their alongshore wavelengths. The main utility of models based on LSA is therefore to identify the physical processes and conditions

Table 3. Bathymetry Surveys Available for the Study

Year	Spring	Summer	Autumn
1998		12 Aug	
1999		07 July	
2000	09 June	31 July	29 Sept
2001	14 June	04 July	17 Oct
2002	05 April	28 July	03 Oct
2003	17 April	09 July	16 Sept
2004		04 Aug	

that might originate a certain bar patch, together with the corresponding time and length scales.

[13] Nonlinear models are used to relax some of the assumptions that are inherent to LSA. They describe situations farther from equilibrium, the predicted patches can be quasiperiodic (with alongshore variability in bar spacing), bars can reach a finite amplitude and waves can vary. However, the existing nonlinear models for formation and development of finger bars are still based on strong assumptions like an alongshore infinite and uniform initial bathymetry and a constant wave field during the model runs [*Caballeria et al.*, 2002; *Garnier et al.*, 2006]. Finally, the timescale of tidal variations is of the same order of finger bar growth time. The cross-shore mobility of the whole inner surf zone during a tidal cycle and the corresponding vertical variations of the sea surface may affect bar development but these effects have been neglected in all the available models.

3. Field Site and Data Set

[14] The field site is located at Noordwijk aan Zee (Netherlands), and is part of the 120-km-long, straight and sandy coast of Holland. The sediment has a median grain size of 0.20 mm. An analysis of annual bathymetric surveys collected since 1964 (JARKUS data set) revealed the presence of two shore-parallel subtidal sand bars over a gentle mean slope of 0.007 [*Wijnberg and Terwindt*, 1995]. These shore-parallel bars often became undulating or crescentic at length scales of hundreds of meters [*van Enckevort and Ruessink*, 2003b].

[15] The wave and tide conditions were measured at the Meetpost Noordwijk (MPN), located 9 km off Noordwijk beach at 18 m water depth. The water level fluctuations were recorded with a 10-min interval and the root mean square wave height, H_{rms}, peak period, T_p, and angle of wave incidence with respect to the shore-normal, θ, were measured every hour. During the study period (1998–2004), the waves had an averaged H_{rms} of 0.76 m and an averaged T_p of 5.7 s. The wave height varied slightly on a seasonal scale, with larger values in fall and winter (October–March, H_{rms} = 0.88 m) than in spring and summer (April–September, H_{rms} = 0.61 m). Waves were mainly obliquely incident, either from NNW ($\theta = 39°$) or from SW ($\theta = -47°$). The semidiurnal tide showed a mean tidal range of 1.4 m at neap tide and of 1.8 m at spring tide. The morphologic boundary condition, defined as the large-scale barred beach configuration, with its local slopes, cross-shore bar spacing and alongshore periodicities, was determined with the use of the JARKUS data set (with measurements around summer) and several extra bathymetries measured in spring and autumn during 2000–2003 (see Table 3).

[16] An Argus video system was used to study the surfzone finger bars [*Holman and Stanley*, 2007]. Five full color cameras were located on the roof of a hotel at 62 m above Mean Sea Level (MSL). They span a 180° view and allow full coverage of 3 km of beach (in the alongshore direction). Finger bars are seen as transverse white stripes (high intensity values) in the time exposure images (averaged over 10 min). The time-exposure images from the five cameras are rectified and merged to a single planview image. The two-dimensional image pixel locations are subsequently transformed into the two-dimensional world coordinates, using photogrammetric relationships where the vertical coordinate is assumed to be equal to the free surface elevation measured offshore [*van Enckevort and Ruessink*, 2003a]. Nearly 6 years of data were used in the present study, from 1 October 1998 until 31 July 2004. Most of the time the cameras worked properly: only 10 technical interruptions of less than 9 days and one interruption of 49 days occurred in June–July 2003 (in total, 2012 days were studied).

4. Methodology

4.1. Planview Images

[17] Time-exposure planview images were automatically collected every daylight hour using a grid of 1 m × 1 m. The ground coordinates had the origin at the Main Beach Pole of km 82.00, located in the dunes nearly in front of the hotel with the cameras. The cameras were located 72 m inshore and 168 m southward of the Pole. The cross-shore coordinate, x, increased seaward and the alongshore coordinate, y, increased southward. At midbeach, the ground accuracy of the planview images was typically 1 m and 2 m in the x and y directions, respectively, but it declined with increasing distance from the cameras. The study was limited to the area where the pixel size was at least 10 times smaller than the dimensions of the features of interest. The study area in Noordwijk had an alongshore extension of 2 km, with the cameras at the center, and a cross-shore extension of 350 m (see Figure 1).

[18] The most conspicuous element of the planview images of Noordwijk was the foam created by predominant wave breaking over the underlying subtidal morphology. Transverse stripes of white foam attached to the low-tide coastline were identified in some images (see Figure 1). They resembled the transverse white bands detected by *Konicki and Holman* [2000] (called "trough bars") and we assumed that they corresponded to bathymetric transverse finger bars. We also observed white stripes at the seaward side of the shore-parallel inner bar (named "offshore bars" by *Konicki and Holman* [2000]), but they occurred less frequently and were more irregular. The data set of the present study was based on the finger bars attached to the low-tide shoreline.

4.2. Selection of Bar Events

[19] The procedure to quantify finger bar properties started by selecting the days with candidate images: those where at least two transverse white stripes could be identified in the planview images. This step was done by visual observation of daily images of the 6 years taken at daylight low-tide hours. Then an objective test was developed to
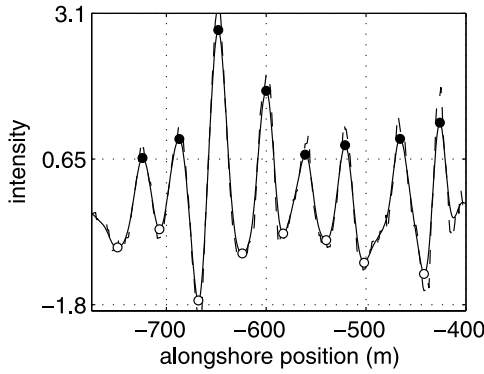
Figure 2. Intensity transect corresponding to the bar patch found in Noordwijk on 27 August 2002, at 1300 GMT. Dashed line, detrended image intensity $\hat{I}$ of an alongshore transect located at $y = [-775, -400]$ m and $x = 180$ m; solid line, low-pass filtered image intensity, I, with detected peaks (solid circles) and valleys (open circles).

detect automatically the crests and troughs of the finger bars in the candidate images. The test was based on finding significant peaks and valleys in the image intensity along an alongshore transect that crosses the transverse white stripes.

[20] Two preprocessing steps were applied before the bar characteristics and dynamics were derived from the intensity transects. First, each intensity transect was normalized and detrended. Then, a matrix $\hat{I}(t, y)$ was constructed containing the detrended image intensity $\hat{I}$ sampled at time t (with 1-hour step) and alongshore position y (with 1-m step). The dashed line in Figure 2 corresponds to the intensity $\hat{I}$ of a transect located at $y = [-775, -400]$ m and $x = 180$ m on 27 August 2002, at 1300 GMT (i.e., over the bar patch shown in Figure 1). Afterward, a low-pass filter that preserved length scales larger than 5 m was applied. We determined the locations of all the peaks and valleys from the resulting low-pass filtered intensity matrix, $I(t, y)$, with the constraint that the intensity difference between consecutive peaks and valleys verified $I_{diff} > (\bar{I} + 0.4\ \sigma_I)$. Here $\bar{I}$ and σ_I are the mean and standard deviation of I in the corresponding transect. This constraint was imposed to ensure that small and short-lived wobbles were not detected as finger bars. The solid line in Figure 2 shows an example of low-pass filtered intensity, I, with the corresponding peaks and valleys.

[21] We identified a bar event when a certain bar patch with at least 3 bars could be continuously detected in a similar position over several subsequent days (at least 2). Well-developed bar events were those involving more than 16 bars in total (during the whole event duration). The objective test yielded the statistics of occurrence of bar patches, bar events and well-developed bar events. The success of the bar detection method not only depended on bar presence but also on image conditions (fog or rain forbid detection) and on wave and tide conditions. Incoming waves did not break on the bars when wave heights were too low or when the tidal water levels were too high. The procedure to detect bars always involved low-tide images and the threshold of wave height for bar detection in such conditions was found to be $H_{rms} = 0.35$ m. The days with

good data for observation of bars, N_{day}^{con}, were those with at least three good images during low-tide and a daily-averaged $H_{rms} > 0.35$ m. The objective test also yielded the percentage of time with bar presence among the time with good data, $P_{tim}^{eve} = 100\ N_{day}^{eve}/N_{day}^{con}$, where N_{day}^{eve} is the number of days with bar events.

4.3. Extraction of Bar Characteristics

[22] We used the images of the three daylight hours closest to low tide to calculate the corresponding wavelength and migration rate on days with bar patches. We thus discarded the images where wave breaking was absent owing to high water levels, but we still averaged out part of the hourly fluctuations of the breaker positions. Three hourly wavelengths, λ_h, were calculated as the alongshore average of the distances between peaks and the distances between valleys in the corresponding low-pass filtered intensity transect, $I(t, y)$ (the standard deviation, σ_{λ_h}, was also kept). The daily wavelength, λ_d, and the corresponding standard deviation, σ_{λ_d}, were obtained by averaging all the distances in the three low-tide daily transects. We also computed the event-averaged wavelength, λ_e, and the standard deviation, σ_{λ_e}. The coefficient of variation of λ was defined as the standard deviation divided by the mean. The cross-shore span of the bar crests (bar elongation, Δx) and the orientation of the crests with respect to the shore-normal were measured manually in a planview image of each well-developed bar event.

[23] Daily alongshore migration rates, c_m, were evaluated during well-developed bar events with a cross-correlation analysis. We averaged over time three low-tide intensity transects of each day with a bar patch, and then we cross-correlated each pair of adjacent daily-averaged transects. The magnitude of the lag at the positive largest peak of the cross-correlogram equaled the alongshore distance that a bar patch migrated between two observations. The sign of this lag indicated the migration direction. We did not compute bar migration when the time gap between two subsequent observations exceeded 48 hours and we only used the rates with a maximum value of the cross-correlogram above 0.7. All the results included in the data set were checked to be insensitive to variations of the methodological parameters.

4.4. Analysis of Wave Conditions and Bathymetries

[24] The alongshore component of the wave radiation stresses, S_{xy}, is an indication of the induced nearshore alongshore current. We computed it with the hourly measured wave conditions of the offshore buoy using the expression,

$$S_{xy} = \frac{\rho g}{16} H_{rms}^2 \sin \theta \cos \theta \quad . \tag{1}$$

[25] Here ρ is the water density and g is the gravitation acceleration. In deep water S_{xy} is proportional to the alongshore component of the wave power, which was used as a proxy for the mean flow along the inner bar by *van Enckevort and Ruessink* [2003b]. We computed the daily mean tide and wave conditions of the entire data set by averaging over the 24 hours prior to each video observation.

[26] We extracted eight successive cross-shore profiles, separated 250 m alongshore, from the bathymetries avail-
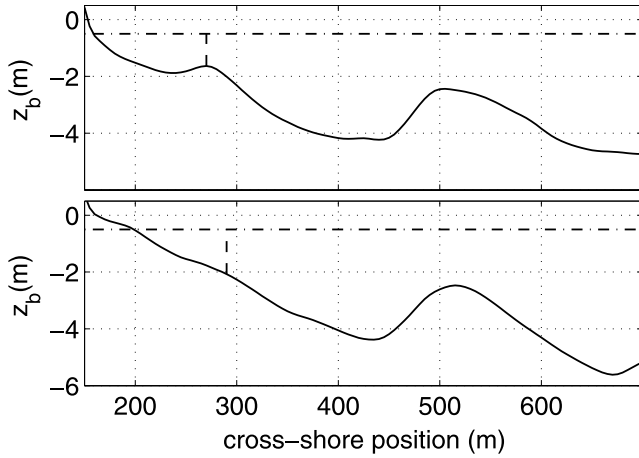
Figure 3. Examples of Noordwijk profiles extracted from the bathymetries, where z_b is the bed level and the horizontal dash-dotted line is the reference low-tide level ($z_s^{lt} \sim -0.5$ m). (top) Profile measured on 3 October 2002, at $y = -500$ m. The vertical dashed line indicates the inner bar crest position. Here $A_t = 117$ m^2 and $\beta_{inn} = 0.021$. (bottom) Profile measured on 29 September 2000, at $y = 750$ m. The vertical dashed line is a reference position verifying $z_b \sim -2$ m. Here $A_t = 85$ m^2 and $\beta_{inn} = 0.020$.

able in the period 1998–2004 (see Table 3). Two examples of profiles are plotted in Figure 3. The low-tide coastline was computed using a reference low-tide level of $z_s^{lt} \sim -0.5$ m for all profiles (horizontal dash-dotted line in the graphs of Figure 3) and we also identified the position of the shore-parallel inner bar crest (vertical dashed line in the top panel). Subsequently, we defined the cross-shore trough area, A_t, as the area between the bottom level, the low-tide level and the vertical line over the inner bar crest. Some profiles, like the one shown in the bottom plot of Figure 3, did not display a shore-parallel inner bar. In these cases, A_t was assumed to be the area bounded by the bottom level, the low-tide level and a vertical line at $z_b \sim -2$ m (vertical dashed line in that plot). We finally defined the slope of the inner surf zone, β_{inn}, as the average of the bed slope across a transect extending from the low-tide shoreline position to 50 m offshore.

[27] Each detected finger bar event was coupled to the nearest cross-shore profile of the bathymetric survey closest in time. We assigned the bathymetric parameters A_t and β_{inn} to the event only if the video observations occurred within 2 months of a bathymetric survey. The bed level of the inner surf zone would change significantly over longer periods. As an example, we did not assign bathymetric parameters to the events occurring between 12 October 1998 and 7 May 1999, for instance (see Table 3).

5. Results

5.1. Description of a Well-Developed Bar Event

[28] A well-developed bar event with a patch of five to eight transverse finger bars occurred from 7 August until 5 October 2002. The bar patch was clearly visible in the planview image of 27 August (see Figure 1) and reappeared in the images whenever $H_{rms} > 0.35$ m (this occurred 34 days). The intensity transect of 27 August at 1300 GMT,

with eight peaks and eight valleys, is shown in Figure 2. The bars in thistransect were regularly spaced, with $\lambda_h = 43$ m, $\sigma_{\lambda_h} = 7$ m and a coefficient of variation of 16%. The white transverse stripes in the planview image of Figure 1 extended about 60 m in the offshore direction and the bar crests deviated from the shore-normal 32° toward N. The assigned profile is shown in the top plot of Figure 3. The finger bars were located between the low-tide shoreline and the trough of the shore-parallel inner bar.

[29] A space-time diagram (time stack) of the hourly low-pass filtered matrix $I(t, y)$ corresponding to this bar event is shown in Figure 4, together with the hourly offshore measured H_{rms}, T_p, θ (relative to shore-normal, positive values mean waves arriving from NW) and S_{xy} (see equation (1)), and the daily measured λ_d and c_m (positive values mean bars migrating toward S). Red in the time stack corresponds to high-intensity values (peaks) and blue represents low-intensity values (valleys). The horizontal alternations of red and blue thus illustrate the presence of transverse finger bars, and a general temporal shift in the bands (e.g., on 21–23 September) reflects the alongshore migration of bars. Gray horizontal bands indicate missing data due to night hours, days with bad images or days with small waves (no wave breakers over the bars). The horizontal lines in the panels for λ_d and c_m equal σ_{λ_d} and the ground accuracy, respectively (images had an alongshore accuracy of 5 m in this region).

[30] Time stacks allowed for a detailed inspection of the wave conditions before, during and after the detection of bar patches. Extremely mild waves occurred during the month prior to 6 August 2002 ($H_{rms} < 0.35$ m during most of the time). We only observed breaking waves in the images on 27 July and 1 August but no finger bars were distinguishable in the corresponding planviews. Hence we considered that the bar patch emerged on 6 and 7 August. The wave field during these two days was quite regular, with mild waves of $H_{rms} = 0.43$ m and persistent oblique incidence from the NNW, $\theta = 50°$ (see Figure 4). The bar patch was "up-current oriented" because the crests deviated toward N whilst alongshore current flowed toward S. The angle of wave incidence remained large during the days when patches were detected and H_{rms} was always below 1.5 m. The event-averaged wave conditions were $H_{rms} = 0.72$ m, $T_p = 5.6$ s and $\theta = 24°$. No bar patches were detected from 6 October until the end of 2002, even though $H_{rms} > 0.35$ m most of the time. The storm on 5 and 6 October, with 2-day averaged $H_{rms} = 1.24$ m and $\theta = 22°$, almost destroyed the bar patch. The planview of 6 October showed three finger bars, but the corresponding intensity transect was already too irregular to define it as a rhythmic bar patch. These remaining bars were finally wiped out in the next storm of that month.

[31] The daily-averaged wavelength was rather constant during the two months, ranging from 40 to 53 m (sixth plot in Figure 4). The event-averaged values were $\lambda_e = 46$ m, $\sigma_{\lambda_e} = 12$ m with a variation coefficient of 26%. The bar patch migrated alongshore with daily rates between -9 and 22 m/day. The sign changed several times and the event average was 3.2 m/day. A qualitative comparison of the fifth and seventh plots in Figure 4 revealed a positive alignment between S_{xy} and c_m. The sign of θ was chosen such that incoming waves from NW (SW) resulted in a positive
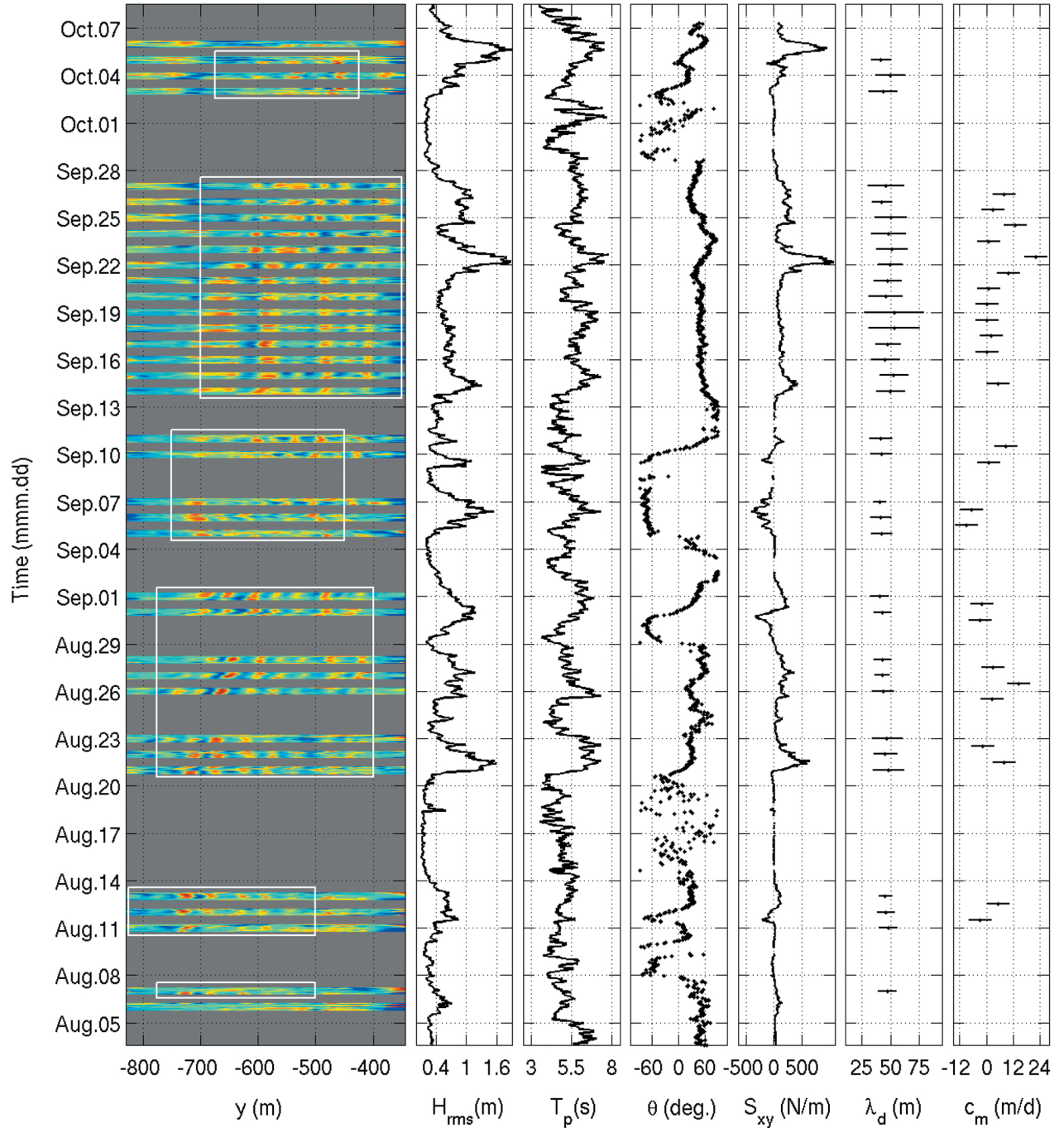
Figure 4. Time series corresponding to the bar event detected from 7 August 7 until 5 October 2002. From left to right: low-pass filtered intensity transects $I(t, y)$ (time stack), hourly offshore measured H_{rms}, T_p, θ (with respect to the shore-normal, positive values mean waves arriving from the NW), and S_{xy}, and daily measured λ_d and c_m (positive values mean migration toward S). In the time stack, red corresponds to high-intensity values (peaks) while blue represents low-intensity values (valleys). Gray horizontal bands correspond to missing data. The horizontal lines in the λ_d and c_m plots correspond to $\pm\sigma_{\lambda_d}$ and the ground accuracy, respectively.

(negative) value of S_{xy}. These waves often resulted in a positive (negative) c_m value. Finally, the finger bar patch showed some temporal changes in shape where two bars merged into one. This occurred twice in the second half of September 2002.

5.2. Occurrence and Duration of Bar Events

[32] We analyzed a total number of 2012 days during the 6 years of observations, after excluding the periods without images due to technical problems. Among them, 1417 days had $H_{rms} > 0.35$ m and were used to detect bars. Transverse
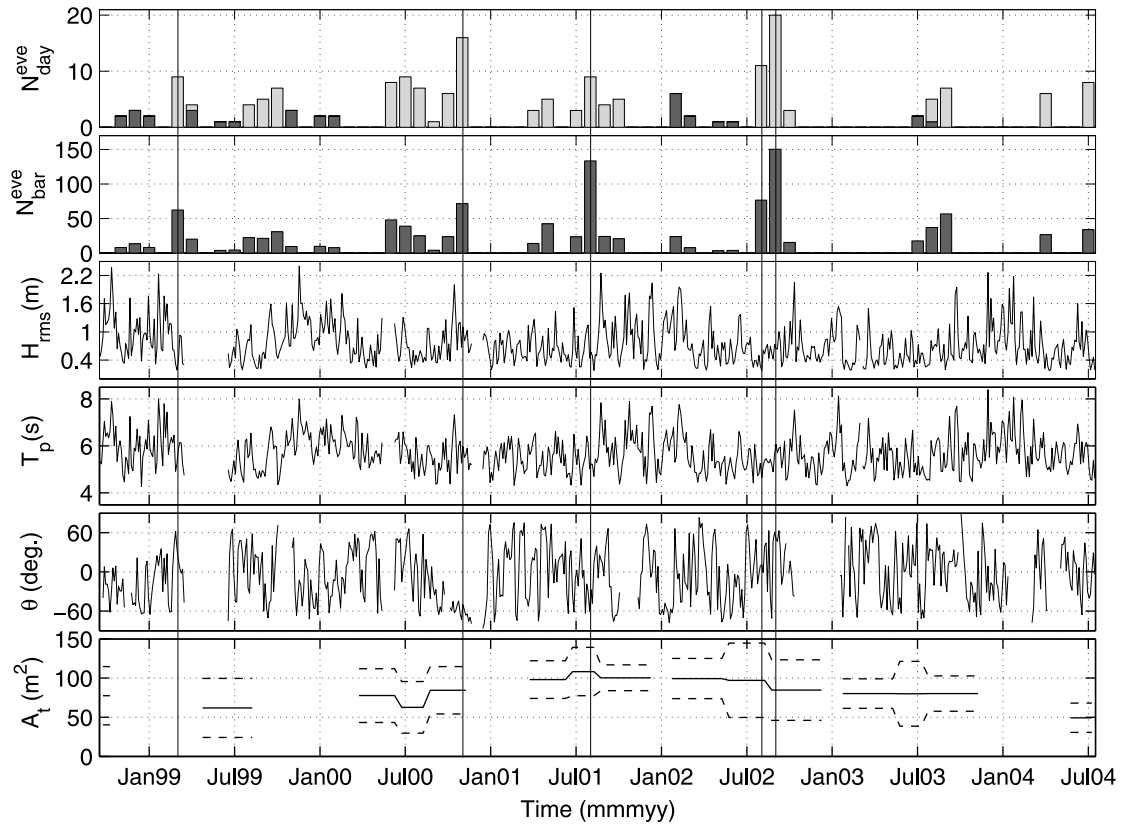
Figure 5. Monthly variability of (from top to bottom) the number of days with bar patches, N_{day}^{eve}, the number of detected bars, N_{bar}^{eve}, the 3-day averaged wave conditions (H_{rms}, T_p and θ), and the trough area of the underlying bathymetries, A_t. In the top plot, the light part of the bars indicates the percentage of days related to well-developed events. In the bottom plot, the solid line is the alongshore-averaged A_t and the two dashed lines are the average plus and minus 1 standard deviation, respectively. Vertical solid lines reflect the 5 months with an over-average bar patch presence.

finger bar patches were distinguishable on 193 days, which resulted in bar presence during 14% of the time with good data. These bar patches were gathered in 44 bar events, characterized by an average of 4.9 bars that were visible during 5.3 days, and the total amount of observed bars was 1142. Bar event duration ranged between 2 days and 2 months and the number of bars per patch ranged between 3 and 9. There were 26 well-developed events with a total amount of 957 bars and 162 days (11% of the time with good data). All detected finger bar patches were attached to the low-tide coastline. The majority were located inside the trough of a shore-parallel inner bar but we also observed the finger bars on almost planar unbarred surfzone profiles (see Figure 3 for examples of the two types of profiles).

[33] The annual number of days with bar patches varied from 14 days in 2003 to 51 days in 2000, with an average of 35 days per year. Figure 5 shows the monthly variability of the presence of bar patches. The first plot is a bar histogram with the monthly number of days with bar presence, N_{day}^{eve}. The light part of the bars indicates the percentage of days with well-developed events. The second plot shows the total number of bars detected each month, N_{bar}^{eve}. The next three plots display the 3-day averaged H_{rms}, T_p and θ. The bottom plot in Figure 5 shows the alongshore-

averaged A_t corresponding to the bathymetries assigned to each month. The vertical lines in all the panels were drawn to point at the top 5 months with an over-average presence of well-developed bar events (March 1999, November 2000, August 2001 and August and September 2002). These months coincided with periods of predominantly oblique waves with 3-day averaged H_{rms} between 0.4 and 1 m, and with an alongshore-averaged A_t that exceeded 75 m^2.

5.3. Wave Conditions and Bathymetric Parameters

[34] We used the hourly measured wave data to investigate in more detail whether the bars occurred under specific conditions. Table 4 contains the statistical descriptors of wave conditions during bar presence. The average of H_{rms} was 0.8 m and the mean absolute value of the daily averaged angle was 49°. The frequency histograms of H_{rms} and θ during the 6 years of observations are shown in the top plots of Figure 6. The H_{rms} displayed a distribution skewed toward the lower heights with a tail toward the higher heights. The frequency distribution of θ displayed a weak bimodality around the shore-normal. Histograms of H_{rms} and θ during the days with bars (middle plots of Figure 6) showed that the presence of obliquely incident waves with intermediate heights was a fundamental element for finger bar development. The distribution of H_{rms} was nearly
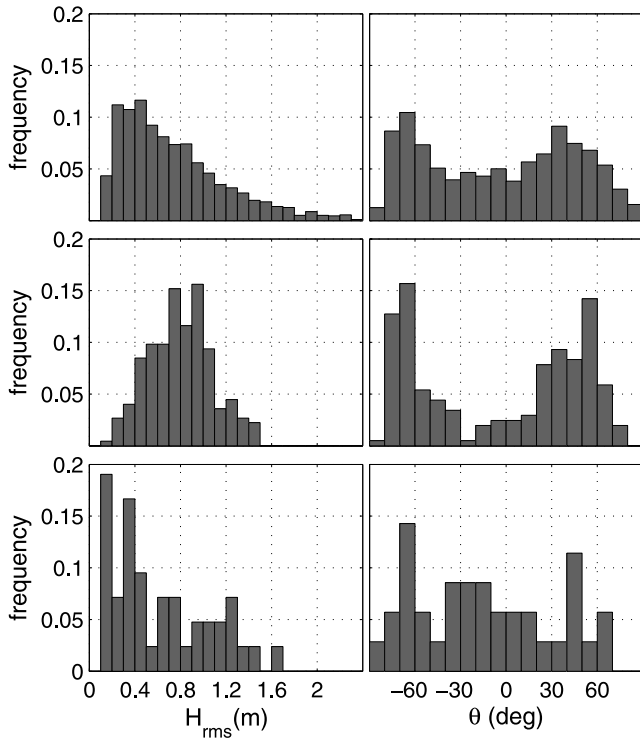
Figure 6. Histograms of daily averaged H_{rms} and θ. (top) Frequency of occurrence during the entire 6 years. (middle) Frequency of occurrence during days with finger bar patches. (bottom) Frequency of occurrence 1 day after the last observation of the events.

symmetric around the maximum at 0.8 m and ranged between 0.25 and 1.5 m, hence the bars did not coexist with high waves. The distribution of θ also differed from the 6-year distribution, since it showed two distinct peaks at $-60°$ and $50°$ and small frequencies of the angles around zero. Finally, we looked to the specific conditions were we lost track of our transverse bars. Frequency histograms of wave conditions one day after the last observation of the events are shown in the bottom plots of Figure 6. Incoming waves of low heights dominated, without any preferred direction of incidence.

[35] We assigned bathymetric parameters to 31 transverse finger bar events, of which 21 were well developed. All other events lacked a bathymetric survey within 2 months of their observation. During bar presence, the mean A_t was
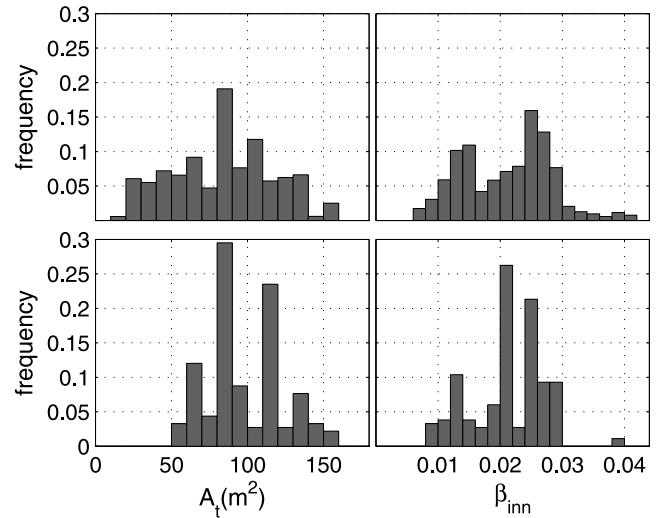

Figure 7. Histograms of the trough area, A_t, and the slope of the inner surf zone, β_{inn}. (top) Frequency of occurrence during the days of the 6 years with a profile assigned. (bottom) Frequency of occurrence during the days with finger bar patch presence and a profile assigned.

95 m^2 and the mean β_{inn} was 0.021 (see Table 4). The frequency histograms of A_t and β_{inn} are shown in Figure 7. The top plots include all the profiles of the bathymetric surveys of the studied period (see Table 3). The data of the profiles assigned to bar events is shown in the bottom plots of Figure 7. We observed that the trough area during bar events always exceeded 50 m^2 and frequency of occurrence was maximum around $80-120$ m^2. The distribution of the inner surf zone slope showed a maximum around 0.02.

5.4. Shape and Dynamics of Bar Patches

[36] The daily averaged wavelength of transverse finger bar patches measured during the 6 years ranged between 21 and 75 m (see Table 4). The average over the entire data set gave $\lambda = 39$ m and $\sigma_\lambda = 13$ m, with a variation coefficient of 32%. The event-averaged wavelength, λ_e, ranged between 22 and 58 m. Figure 8 shows that λ_e increased linearly with an increase of the event-averaged surf zone width, $X_b \propto H_{rms}/\beta_{inn}$, as predicted by some models (see section 2). The β_{inn} could only be accurately estimated in 12 well-developed events, when the finger bars detected in the planviews were located near the low-tide shoreline of the assigned cross-shore profile. This condition

Table 4. Results for the Statistical Descriptors of the Wave Conditions (H_{rms}, T_p, and Absolute Value of θ) During Bar Patch Presence, the Properties of the Profiles (A_t and β_{inn}) During Bar Events, and the Bar Patch Characteristics (λ and Absolute Value of c_m)[a]

Descriptor	H_{rms}, m	T_p, s	$\|\theta\|$, deg	A_t, m^2	β_{inn}	λ, m	$\|c_m\|$, m/d
Daily averaged values: mean	0.80	5.7	49	95	0.021	39	4.5
Daily averaged values: std	0.33	0.8	25	28	0.13	13	3.8
Daily averaged values: max	1.49	7.2	81	156	0.039	75	22.0
Daily averaged values: min	0.18	4.2	2	57	0.009	21	0.0
Event-averaged values: max	1.10	6.4	77	–	–	58	8.6
Event-averaged values: min	0.43	4.8	1	–	–	22	0.0

[a]The mean, the standard deviation, the maximum value, and the minimum value of the daily averaged quantities are given, together with the maximum and minimum values of the event-averaged quantities.
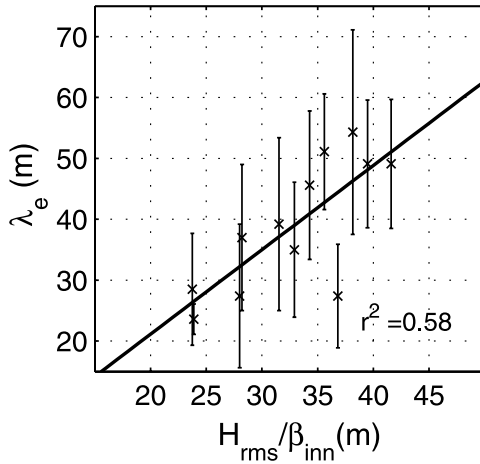
Figure 8. Event-averaged wavelength during the well-developed events with a profile assigned against event-averaged offshore H_{rms} divided by slope of the inner surf zone, β_{inn}. The vertical lines correspond to $\pm\sigma_{\lambda_e}$.

Figure 10. Daily migration rate during well-developed events against daily averaged radiation stresses measured offshore.

ensured that detected bars were located within the cross-shore transect used to calculate β_{inn}. Figure 8 presents the relationship between λ_e and the ratio H_{rms}/β_{inn} for these 12 events. We got a linear relation between the two parameters with a correlation coefficient of $r^2 = 0.58$ (95% confidence level).

[37] We measured a cross-shore extension of the white transverse stripes between 15 and 60 m. The average value was 26 m with a standard deviation of 10 m. The bar crests were mostly shore-oblique, deviating an angle up to 40° from the shore-normal (bar orientation). The average of the absolute value of bar orientation was 20° for the entire data set, with a standard deviation of 12°. Figure 9 illustrates that crest lines pointed toward the direction of incidence of the incoming waves. In that figure, the angle of crest orientation during the well-developed events is plotted against the average of θ measured during 48 hours before the first bar observation. Bars deviating toward N (S) were assigned a positive (negative) value of the bar orientation angle and
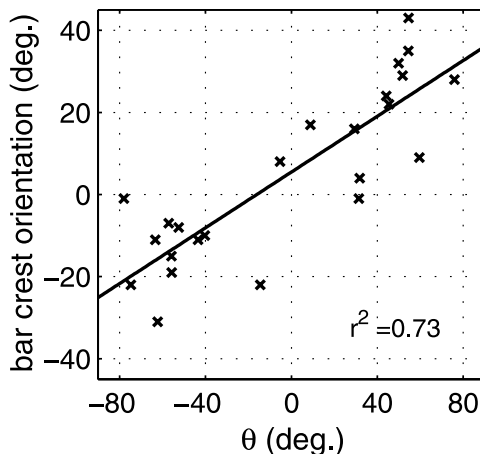
corresponded to waves from N (S). We obtained a linear relation between the wave direction and the bar crest orientation, with a correlation coefficient of $r^2 = 0.73$ (99% confidence level). This showed that bar crests were always oriented against the instantaneous current that was present during their formation ("up-current orientation").

[38] The mean of the absolute values of the daily migration rates was $|c_m| = 4.5$ m/day, with a standard deviation of 3.8 m/day and a maximum of 22 m/day (see Table 4). The event-averaged migration rate was up to 8.6 m/day. The daily values of c_m were plotted against the daily averaged S_{xy} for all the days during well-developed finger bar events. As shown in Figure 10, migration rates increased linearly when S_{xy} increased. We forced a linear relation through the origin because the bars cannot migrate in case of shore-normal waves ($S_{xy} = 0$). The slope of the regression line was 0.020 m²/(N day) and the linear correlation coefficient was $r^2 = 0.65$, highly significant at 99% confidence level (despite its scatter). Since S_{xy} can be used as a proxy of the alongshore current, Figure 10 showed that finger bars certainly migrated in the direction of the current.

6. Discussion

[39] Patches of transverse finger bars were a rather common feature on the subtidal beach of Noordwijk. Both the percentage of time with bar patches and the number of bars in a patch exceeded those detected at Duck beach by *Konicki and Holman* [2000]. Table 5 shows a comparison of the results at the two sites. Many events of initial bar formation and subsequent development were identified at Noordwijk (44 in 6 years). Our analysis of these events allowed for a detailed description of the wave energy conditions before, during and after the detection of the bars, and the properties of the large-scale morphology conditions could also be assessed for many events. These are crucial steps to increase the understanding of the physical mechanisms for growth and evolution of bar patches. Moreover, bar properties were correlated with hydrodynamic and bathymetric parameters, which is essential to test the predictions of existing models.

Figure 9. Angle of bar crest orientation in well-developed events against offshore angle of wave incidence averaged the 48 hours before the bars were observed.
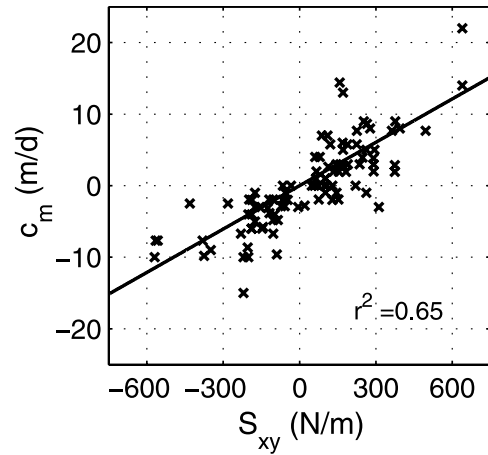
Table 5. Comparison of Finger Bar Patches Detected at Noordwijk Beach With the Trough Bars Detected at Duck Beach by *Konicki and Holman* [2000][a]

	Period	N_{day}^{con}	P_{tim}^{eve}, %	N_{bar}^{pat}	Persistence	λ_d m	Bar Crest Orientation	Migration Velocity
Noordwijk	6 years	1417	14	3–9	<2 months	39 ± 13	20° ± 12°, up-current	<22 m/d, down-flow
Duck	10 years	1477	10	1–4	<3 months	79 ± 38	32° ± 21°, not given	<40 m/d, unclear

[a]N_{day}^{con} is the number of days with good video data, P_{tim}^{eve} is the percentage of time with bar presence among the time with good data, and N_{bar}^{pat} is the number of bars per patch. Bar crest orientation is measured with respect to the shore-normal.

[40] The wave conditions measured during finger bar presence indicated that obliquely incident waves of intermediate and relatively constant height must occur for a few days to permit the formation and persistence of bar patches (see Figure 6). This was in agreement with the vertical lines in Figure 5 that reflected the months with more bars and coincided with periods of intermediate waves and oblique incidence. The wave period did not seem to play any important role. The results for the wave conditions during bar destruction were less conclusive. In most cases, we lost track of the finger bars (no breakers on top owing to wave height decay) before they were destroyed (see the bottom left plot in Figure 6). However, a viable explanation is that large waves wiped out the bars since the latter were never detected when $H_{rms} > 1.5$ m (see the middle left plot in Figure 6). Also, there were no bar patches during the more wave energetic winter months (see Figure 5). No other seasonal tendencies in bar presence could be assessed, probably because finger bar formation not only required certain wave conditions but also specific bathymetric boundary conditions.

[41] Finger bar patches were only observed when the area of the inner bar trough was larger than 50 m^2 (see Figure 7). The bars detected in Duck showed a similar behavior: they occurred more frequently when the inner shore-parallel bar was located farther offshore. *Konicki and Holman* [2000] already pointed out that the presence of a shore-parallel bar close to shore can change the hydrodynamic regime in a way that it prevents the formation of finger bars. In our Noordwijk observations, the trough area was the best indicator for the accommodation space that permitted or prevented the formation of bar patches and the coupled hydrodynamic circulation. Bathymetric indicators influenced not only the monthly variability of bar occurrence but also the alongshore location of bar patches and the number of bars in one patch on one day. Bar patches were often observed in specific regions of some 200–500 m within the alongshore rhythmic morphologies of the shoreline and the inner nearshore bar at Noordwijk (see Figure 1). An optimal trough area (around 100 m^2) and an optimal slope of the inner surf zone (around 0.02) were more conducive to bar formation.

[42] The mean wavelength of the transverse finger bar patches detected in Noordwijk was half the size of that reported at Duck site (see Table 5). Alongshore distances measured between bars in one patch were rather homogeneous in the present data. The coefficient of variation of the daily averaged wavelengths in the entire data set was 32% for the bars in Noordwijk and 48% for those in Duck (i.e., bars were more regularly spaced in Noordwijk). The alongshore ground accuracy in planview images (2–8 m in

Noordwijk) could explain about 15% of the alongshore variability in the present study. Bar crests extended in the cross-shore direction up to 60 m, a distance similar to that of Duck bars. As underlined by *Konicki and Holman* [2000], the measurements of the cross-shore elongation of the foam stripes probably underestimated the real length of topographic bars since when they entered deeper locations no visible breaking could be detected. The angle of deviation of detected bar crests with respect to the shore-normal was also similar in both sites. In the present study, the angle of wave incidence averaged during 48 hours before the beginning of each bar event was correlated with the bar crest orientation (see Figure 9). Finger bar crests were pointing toward the incoming waves, thus bars were "up-current oriented."

[43] A highly significant correlation was established between the bar migration rates and the alongshore component of the radiation stresses. Several reasons could explain the scatter in Figure 10. Some error sources could be associated with the technique for determining c_m from the planview images. The alongshore ground accuracy in the images (2–8 m) was of the order of the mean migration rate. Changes in tidal level and offshore H_{rms} could produce apparent migration of the foam patterns in the images because waves broke in different positions with the same underlying bathymetry [*van Enckevort and Ruessink*, 2003a]. However, the latter effect was probably marginal in our Noordwijk study because bar migration was alongshore (not cross-shore) and we only observed a small range of variation in H_{rms} (<1 m) and in tidal levels (<0.3 m) during bar detection. Processes of merging were observed in a few finger bars events. These processes were not quantified but could also induce errors in migration rate measurements.

7. Comparison With the Predictions of Self-Organization Models

[44] The specific wavelengths, shapes and migration rates measured in Noordwijk and also their relationships with hydrodynamic and bathymetric parameters were compared with model predictions listed in Table 2. Both the range of detected wavelengths (21–75 m) and their linear relation with the surfzone width (see Figure 8) were in line with the predictions of all the model solutions. Thus the length scales of the features were not a relevant quantity to discriminate between processes. Otherwise the large angles of wave incidence measured during finger bar presence (see Figure 6) and the up-current bar crest orientation measured in Noordwijk (see Figure 9) clearly ruled out the bed-surf coupling. Therefore, among the different dominant mechanisms included in Table 2, only the bed-flow coupling

Table 6. Quantitative Comparison Between the Up-Current–Oriented Bars Predicted by Two Self-Organization Models and the Surfzone Bars Detected at Noordwijk (Mean Values)

Reference	θ, deg	β	X_b, m	λ, m	c_m, m/d
Ribas et al. [2003]	50	0.02	50	60	100
Garnier et al. [2006]	25	0.05	20	75	45
Noordwijk bars	49	0.02	40	39	4.5

remained a viable explanation for Noordwijk finger bars. In situ measurements of the suspended sediment concentration over finger bars and the associated currents should be made to verify this conclusion. Regarding bar mobility, Noordwijk observations verified the general model prediction that migration of patches is in the direction of the alongshore current (see Figure 10).

[45] The predictions of two self-organization models that dealt with large angles of wave incidence and predicted the formation of up-current bars were studied in depth [*Ribas et al.*, 2003; *Garnier et al.*, 2006]. A detailed comparison with Noordwijk bars was not possible because both models used an initially planar reference profile, whereas beach profiles in Noordwijk displayed one or two shore-parallel bars. However, since our observations never indicated a strong interaction between the finger bars and the inner bar, model results were compared with the mean values of Noordwijk observations (see Table 6). A LSA was performed by *Ribas et al.* [2003], on the basis of highly idealized formulations for both sediment transport and wave transformation (monochromatic waves were assumed and shoaling effects were neglected). Some of the assumptions of that study were relaxed by *Ribas et al.* [2005], who included random wave heights and shoaling effects, and up-current bars remained as a robust outcome. The work of *Garnier et al.* [2006] was pioneering in describing finite amplitude finger bar patches using a nonlinear model and oblique wave incidence. They used an idealized sediment transport formula and included the effect of wave height randomness and the refraction of waves by currents and by the growing topography. *Garnier et al.* [2006] only described their results for a few cases (β = 0.05 and θ equal to 0° or 25°). Quantitative examples of the results of these two models for up-current bars are included in Table 6. The predictions were consistent with the mean values of our field observations, with one exception: modeled migration rates were 1 order of magnitude larger than the detected values. Performing a more detailed model-data comparison was not possible because none of the studies used Noordwijk wave and bathymetric conditions.

[46] The hypothesis behind self-organization models limit their comparison with features growing on natural beaches, as explained in section 2. However, the characteristics of the present observations of finger bars in Noordwijk were remarkably in line with the main model assumptions. First, the large-scale bathymetry of Noordwijk evolves so slowly in time (O(years) [see *van Enckevort and Ruessink*, 2003a]) that it can be considered to be in equilibrium during the fast timescales of finger bars, of O(days). Second, bar patches consisted of a significant number of bars (4–9 in most well-developed events) with relatively regular alongshore wave-

lengths. Third, wave fields were quite regular during bar formation and evolution. However, in disagreement with model assumptions, Noordwijk beach showed a significant tidal range (~1.6 m). More research must be done to clarify how tidal variability affects finger bar development.

8. Conclusions

[47] We detected surfzone transverse finger bar patches in the inner trough of Noordwijk beach, attached to the low-tide shoreline. A patch of finger bars consisted of 3 to 9 sand bars extending in the offshore direction with an oblique orientation and spaced quasiregular in the alongshore direction ($\lambda \sim 21-75$ m). We identified 44 events of formation and evolution of bar patches, which lasted from 2 days to 2 months. There were 193 days with bar patches (14% of the time) during the 6 years of observations.

[48] The wave conditions during bar presence consisted of regular waves with intermediate heights, $H_{rms} = 0.80$ m, coming from large angles of incidence with respect to the shore-normal (the mean of the absolute value of the daily angle was $|\theta| = 49°$). Waves with larger heights ($H_{rms} > 1.5$ m) or from a shore-normal direction destroyed the bar patches. Bars were absent in winter since large storms prevented their development. There was an over-average presence of bars during periods when the cross-shore trough area between the shoreline and the inner bar crest was large enough to accommodate the finger bars and the associated flow circulation. The alongshore nonuniformities of the barred Noordwijk morphology explained the limited number of bars per patch and their alongshore location. Optimal trough areas (around 100 m^2) and inner surfzone slopes (around 0.02) were more conducive to bar formation.

[49] The mean of the daily averaged wavelength was 39 m with a standard deviation of 13 m (32% of wavelength variability). Results indicated that the event-averaged wavelength increased linearly with increasing H_{rms}/β_{inn}. The detected bar crests extended from 15 to 60 m into the surf zone and deviated from the shore-normal up to 40° against the alongshore current (up-current orientation). Bar patches migrated in the direction of the alongshore current at rates up to 22 m/day (the mean rate was 4.5 m/day).

[50] We compared the video observations with results of self-organization models to gain understanding about the physical mechanisms leading to bar development. Our observations ruled out the bed-surf coupling but not the bed-flow coupling as a feasible cause of these bars. The deflection of the alongshore current created by the growing up-current bars could produce enough feedback to the sand transport to explain the existence of finger bar patches in Noordwijk. Predictions of two models that included the bed-flow coupling were subsequently compared quantitatively with the data. The shape and wavelength were consistent but less agreement was found in bar migration. The direction was correctly predicted but the values were 1 order of magnitude larger in the models.

References

Caballeria, M., G. Coco, A. Falqués, and D. A. Huntley (2002), Self-organization mechanisms for the formation of nearshore crescentic and transverse sand bars, *J. Fluid Mech.*, *465*, 379–410.

Calvete, D., N. Dodd, A. Falqués, and S. M. van Leeuwen (2005), Morphological development of rip channel systems: Normal and near normal wave incidence, *J. Geophys. Res.*, *110*, C10006, doi:10.1029/2004JC002803.

Christensen, E., R. Deigaard, and J. Fredsoe (1995), Sea bed stability on a long straight coast, in *Coastal Engineering 1994*, vol. 4, edited by B. L. Edge, pp. 1865–1879, Am. Soc. of Civ. Eng., New York.

Eliot, M. J., A. Travers, and I. Eliot (2006), Morphology of a low-energy beach, Como Beach, Western Australia, *J. Coastal Res.*, *22*(1), 63–77.

Garnier, R., D. Calvete, A. Falqués, and M. Caballeria (2006), Generation and nonlinear evolution of shore-oblique/transverse sand bars, *J. Fluid Mech.*, *567*, 327–360.

Gelfenbaum, G., and G. R. Brooks (2003), The morphology and migration of transverse bars off the west-central Florida coast, *Mar. Geol.*, *200*, 273–289.

Holman, R. A., and J. Stanley (2007), The history and technical capabilities of Argus, *Coastal Eng.*, *54*(6–7), 477–491.

Holman, R. A., G. Symonds, E. B. Thornton, and R. Ranasinghe (2006), Rip spacing and persistence on an embayed beach, *J. Geophys. Res.*, *111*, C01006, doi:10.1029/2005JC002965.

Klein, M. D., and H. M. Schuttelaars (2005), Morphodynamic instabilities of planar beaches: Sensitivity to parameter values and process formulations, *J. Geophys. Res.*, *110*, F04S18, doi:10.1029/2004JF000213.

Komar, P. D. (1998), *Beach Processes and Sedimentation*, 2nd ed., Prentice-Hall, Upper Saddle River, N. J.

Konicki, K. M., and R. A. Holman (2000), The statistics and kinematics of transverse bars on an open coast, *Mar. Geol.*, *169*, 69–101.

Niederoda, A. W., and W. F. Tanner (1970), Preliminary study on transverse bars, *Mar. Geol.*, *9*, 41–62.

Ribas, F., A. Falqués, and A. Montoto (2003), Nearshore oblique sand bars, *J. Geophys. Res.*, *108*(C4), 3119, doi:10.1029/2001JC000985.

Ribas, F., N. Vis-Star, H. Swart, and A. Falqués (2005), Generation of nearshore oblique sand bars: Sensitivity to sand transport formulation, in *Coastal Engineering 2004*, vol. 3, edited by J. M. Smith, pp. 2888–2900, World Sci., Singapore.

van Enckevort, I. M. J., and B. G. Ruessink (2003a), Video observations of nearshore bar behaviour. Part 1: Alongshore uniform variability, *Cont. Shelf Res.*, *23*, 501–512.

van Enckevort, I. M. J., and B. G. Ruessink (2003b), Video observations of nearshore bar behaviour. Part 2: Alongshore non-uniform variability, *Cont. Shelf Res.*, *23*, 513–532.

van Leeuwen, S. M., N. Dodd, D. Calvete, and A. Falqués (2006), Physics of nearshore bed pattern formation under regular or random waves, *J. Geophys. Res.*, *111*, F01023, doi:10.1029/2005JF000360.

Wijnberg, K. M., and J. H. J. Terwindt (1995), Extracting decadal morphological behavior from high-resolution, long-term bathymetric surveys along the Holland coast using eigenfunction analysis, *Mar. Geol.*, *126*, 301–330.

Wright, L. D., and A. D. Short (1984), Morphodynamic variability of surf zones and beaches: A synthesis, *Mar. Geol.*, *56*, 93–118.

———————————

A. Kroon, Geografisk Institut, Københavns Universitet, Øster Voldgade 10, DK-1350 København K, Denmark. (ak@geogr.ku.dk)

F. Ribas, Institut de Ciències del Mar, CSIC, Passeig Marítim de la Barceloneta 37-49, E-08003 Barcelona, Spain. (ribas@cmima.csic.es)